

Durham Research Online

Deposited in DRO:

25 July 2014

Version of attached file:

Accepted Version

Peer-review status of attached file:

Peer-reviewed

Citation for published item:

Mathias, S.A. and McElwaine, J.N. and Gluyas, J.G. (2014) 'Heat transport and pressure buildup during carbon dioxide injection into depleted gas reservoirs.', *Journal of fluid mechanics.*, 756 . pp. 89-109.

Further information on publisher's website:

<http://dx.doi.org/10.1017/jfm.2014.348>

Publisher's copyright statement:

© Cambridge University Press 2014 The online version of this article is published within an Open Access environment subject to the conditions of the Creative Commons Attribution licence
<<http://creativecommons.org/licenses/by/3.0/>>.

Additional information:

Use policy

The full-text may be used and/or reproduced, and given to third parties in any format or medium, without prior permission or charge, for personal research or study, educational, or not-for-profit purposes provided that:

- a full bibliographic reference is made to the original source
- a [link](#) is made to the metadata record in DRO
- the full-text is not changed in any way

The full-text must not be sold in any format or medium without the formal permission of the copyright holders.

Please consult the [full DRO policy](#) for further details.

Heat transport and pressure buildup during carbon dioxide injection into depleted gas reservoirs

Simon A. Mathias¹†, Jim N. McElwaine¹, Jon G. Gluyas¹

¹Department of Earth Sciences, Durham University, Durham, UK

(Received 2014-01-??)

In this article, a two-layer vertical equilibrium model for the injection of CO₂ into a low pressure porous reservoir containing methane and water is developed. The dependent variables solved for include pressure, temperature and CO₂-CH₄ interface height. In contrast to previous two-layer vertical equilibrium models in this context, compressibility of all material components is fully accounted for. Non-Darcy effects are also considered using the Forchheimer equation. The results show that, for a given injection scenario, as the initial pressure in the reservoir decreases, both the pressure buildup and the temperature change increase. A comparison was conducted between a fully coupled non-isothermal numerical model and a simplified model where fluid properties are held constant with temperature. This simplified model was found to provide an excellent approximation when using the injection fluid temperature for calculating fluid properties, even when the injection fluid was as much as $\pm 15^\circ\text{C}$ of the initial reservoir temperature. The implications are that isothermal models can be expected to provide useful estimates of pressure buildup in this context. Despite the low viscosity of CO₂ at the low pressures studied, non-Darcy effects were found to be of negligible concern throughout the sensitivity anal-

† Email address for correspondence: s.a.mathias@durham.ac.uk

22 ysis undertaken. This is because the CO₂ density is also low in this context. Based on
23 these findings, simplified analytic solutions are derived, which accurately calculate both
24 the pressure buildup and temperature decline during the injection period.

25 1. Introduction

26 The potential for storing CO₂ in geological reservoirs continues to attract the atten-
27 tion of national greenhouse gas emission reduction strategies around the world. Reservoir
28 types under consideration include saline aquifers, depleted oil reservoirs and depleted gas
29 reservoirs. Saline aquifers have the advantage of being ubiquitous across the world (Ben-
30 tham & Kirby 2005). However, depleted oil and gas reservoirs are often heralded due
31 to advantages associated with better levels of current characterization (due to previous
32 oil and gas production) and reduced uncertainty associated with the cap-rock integrity
33 (the trap mechanism has already been demonstrated through the presence of hydro-
34 carbon product originally deposited millions of years earlier) (Loizzo *et al.* 2009). Many
35 depleted gas reservoirs have the added advantage of exceptionally low abandonment pres-
36 sures along with highly compressible formation fluids (gas as opposed to oil and water).
37 Estimated CO₂ storage capacities for depleted gas reservoirs have been found to be as
38 much as 13 times higher than those estimated for saline aquifers of equivalent geometries
39 (Barrufet *et al.* 2010).

40 Gas reservoirs within the UK continental-shelf are typically located between 700 m
41 and 3600 m below sea level (Gluyas & Hitchens 2003). Reservoir net-thicknesses range
42 from 20 m to 300 m with gas saturations, fairly uniformly distributed within the reservoir
43 units, representing between 50% and 85% of the available pore-space (Gluyas & Hitchens
44 2003). The remainder of the pore-space is generally filled with residually trapped brine.

45 Reservoir geometries vary considerably, with the most common being domes or gently
46 titled slabs, covering regions of up to 250 km² (Gluyas & Hichens 2003).

47 Prior to production, gas reservoirs typically exhibit pressures at or above hydrostatic
48 pressure (generally greater than 10 MPa). Many such reservoirs are highly compartmen-
49 talized, exhibiting poor levels of aquifer influx. Consequently, at abandonment, reser-
50 voir pressures are often found to be close to atmospheric conditions. Around the world,
51 gas reservoir abandonment pressures commonly range between 0.35 and 0.8 MPa (Mac-
52 Roberts 1962; Okwananke *et al.* 2011). Note that in compartmentalized reservoirs, gas
53 saturations tend to change very little following reservoir depletion, due to the increase
54 in gas volume associated with the pressure decline.

55 A number of recent simulation studies have discussed the interesting thermal effects
56 that develop as a consequence of CO₂ injection into geological reservoirs. These include
57 cooling due to expansion, heating due to compression, heating and cooling due to disso-
58 lution and vaporization, respectively, differences in temperature associated with injection
59 and reservoir fluids and heating due to viscous heat dissipation (Oldenburg 2007; Andre
60 *et al.* 2010; Han *et al.* 2010). Due to the Joule-Thomson coefficient of CO₂ being larger at
61 lower pressures, such processes are likely to be of greater significance in low pressure de-
62 pleted gas reservoirs as opposed to hydrostatic or over-pressured saline aquifers (Mathias
63 *et al.* 2010).

64 Most previous simulation work relating to CO₂ storage has focused on pressures greater
65 than 10 MPa (e.g. Andre *et al.* 2010; Mathias *et al.* 2013a). Exceptions to these include
66 Han *et al.* (2012) who considered a minimum initial pressure of 6.89 MPa, Ziabaksh-Ganji
67 & Kooi (2014) who assumed an initial pressure of 6 MPa, Afanasyev (2013) who assumed
68 a minimum initial pressure of 4.5 MPa and Singh *et al.* (2011, 2012) who considered
69 an initial pressure of 4 MPa. However, depleted gas reservoirs are often abandoned at

70 pressures lower than 1 MPa. Mukhopadhyay *et al.* (2012) presented numerical simulations
71 concerning CO₂ injection into a depleted gas reservoir at 0.5 MPa. However, they ignored
72 thermal effects and considered the reservoir to be of infinite extent. This study seeks
73 to explore the importance of heat transport coupling on pressure buildup estimation
74 during CO₂ injection in low pressure depleted gas reservoirs. Furthermore, non-Darcy
75 effects associated with high velocities around the injection well are incorporated using
76 the Forchheimer equation.

77 Significant temperature changes are most likely to occur when pressure gradients (in
78 time and space) are sharpest. This will mostly be the case during the injection period.
79 Consequently, although many previous CO₂ storage studies have studied the long periods
80 of time after CO₂ injection has ceased (e.g. Hesse *et al.* 2007, 2008; MacMinn *et al.* 2010,
81 2011), here it is pertinent only to consider the time prior to injection ceasing.

82 The outline of this article is as follows: Firstly, the governing equations concerning
83 mass conservation are presented for a system whereby pure CO₂ is injected into a low
84 pressure closed reservoir containing CH₄ and residually trapped water. Expressions for
85 vertically integrated fluxes are derived following the adoption of the Forchheimer equation
86 along with an assumption of vertical equilibrium. A corresponding energy conservation
87 statement is presented. Details of the solution procedure are provided followed by details
88 concerning the obtaining of relevant thermodynamic properties. Further insight is then
89 sought by the deriving of simplified analytic solutions for heat transport and pressure
90 buildup. A sensitivity analysis is then conducted to explore the role of initial pressure and
91 heat flow coupling on pressure buildup during CO₂ injection into low pressure depleted
92 gas reservoirs. Finally the article summarizes and concludes.

93 2. The mathematical model

94 Consider a fully penetrating vertical injection well of radius, r_w [L], located at the cen-
 95 ter of a horizontally oriented, homogeneous and isotropic, confined cylindrical reservoir
 96 of thickness, H [L], and radial extent, r_e [L]. Four material components are considered
 97 and referenced by the subscript, i , which takes the values c for CO₂, m for CH₄, w for
 98 water and r for rock. A mixture theory is assumed such that all components are consid-
 99 ered to exist at every point in space with some volume fraction, θ_i . The four material
 100 components must satisfy the volume constraint $\sum_i \theta_i = 1$.

101 The reservoir is initially filled with CH₄ alongside a uniform residual saturation of
 102 water with volume fraction, θ_w [-]. The H₂O is assumed to be residually trapped and
 103 immobile such that $\theta_w \rho_w$ is constant (Singh *et al.* 2011, 2012). The volume fraction of
 104 the rock is $\theta_r = 1 - \phi$, where ϕ [-] is the porosity, and the product $\theta_r \rho_r$ is also constant.
 105 The compressibility of all components is allowed for although, as shown later, in the
 106 context of this study, the compressibility and thermal expansion of the water and rock
 107 are negligible due to the relatively small pressure and temperature changes involved.

108 The CO₂ is injected at the origin at a constant mass flow rate, M_0 [MT⁻¹]. Although
 109 the CO₂ and CH₄ are miscible (Ren *et al.* 2000), for simplicity, dispersion and mixing of
 110 the two components are ignored and a sharp interface is assumed, located at an elevation
 111 of h_c [L] above the base of the reservoir (similar to Nordbotten & Celia 2006). At 35°C,
 112 for pressures ranging between 0.7 MPa and 15 MPa, the densities of CO₂ and CH₄ range
 113 between 12 kg/m³ to 815 kg/m³ and 4 kg/m³ to 111 kg/m³, respectively (Lemmon *et*
 114 *al.* 2013). The ranges of corresponding dynamic viscosities for CO₂ and CH₄ are 15.5
 115 μ Pa s to 73.6 μ Pa s and 11.6 μ Pa s to 16.2 μ Pa s, respectively (Lemmon *et al.* 2013).
 116 Because the CO₂ is denser than the CH₄, h_c represents the thickness of the CO₂ layer.
 117 The thickness of the CH₄ layer is then $h_m = H - h_c$.

118 Let us denote $P(r, t)$ [$\text{ML}^{-1}\text{T}^{-2}$] and $T(r, t)$ [Θ^{-1}] as the pressure and temperature at
 119 the location of the CO_2 - CH_4 interface, respectively, where r [L] is the horizontal radial
 120 distance from the center of the injection well and t [T] is time after commencement of
 121 injection.

122 In most cases of physical interest, $r_e \gg H$, so it is convenient to make a shallowness
 123 assumption (Nordbotten & Celia 2006; Hesse *et al.* 2007, 2008; MacMinn *et al.* 2010,
 124 2011). This can be rigorously derived as an expansion in $H/r_e \ll 1$, but the result is
 125 equivalent to assuming vertical equilibrium. It is therefore assumed that the temperature
 126 is uniform vertically and identical in the rock, CO_2 , CH_4 and water. The densities ρ_i
 127 [ML^{-3}] for each fluid species are also assumed to be constant vertically and given by
 128 the equation of state evaluated at the interface, that is using P and T . The vertical
 129 momentum equation is then simplified by assuming an equilibrium between gravity and
 130 hydrostatic pressure such that (Hesse *et al.* 2007)

$$P(r, z, t) = \begin{cases} P(r, t) + \rho_c g(h_c - z), & 0 \leq z \leq h_c, \\ P(r, t) + \rho_m g(h_c - z), & h_c < z \leq H, \end{cases} \quad (2.1)$$

131 where P [$\text{ML}^{-1}\text{T}^{-2}$] is the local pressure, ρ_c [ML^{-3}] and ρ_m [ML^{-3}] are the densities
 132 of CO_2 and CH_4 , respectively, g [LT^{-2}] is gravitational acceleration and z [L] is the
 133 height above the base of the reservoir. After depth integrating, the primary dependent
 134 variables of our model then become $P(r, t)$, $T(r, t)$ and $h_c(r, t)$. Some general features of
 135 the conceptual model are illustrated further in Figure 1.

136 Note that assuming the fluids are incompressible, ignoring heat transport and tem-
 137 perature changes and ignoring the density difference between the different components,
 138 such a problem reduces to the classic Buckley & Leverett (1942) equation, where rela-
 139 tive permeability is assumed to be a linear function of h_c and h_c is equivalent to fluid
 140 saturation.

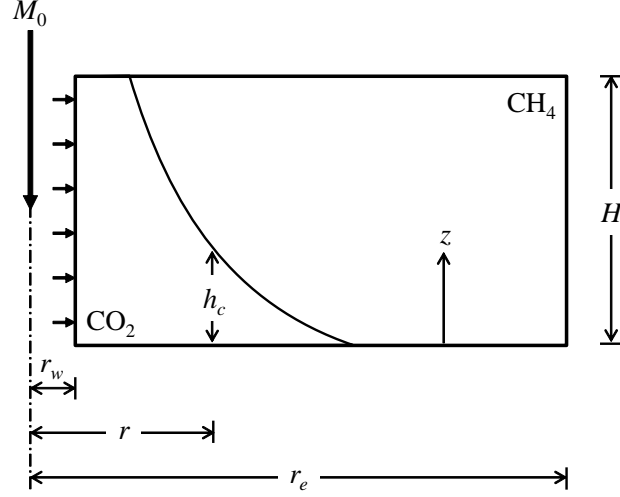


FIGURE 1. Schematic diagram of conceptual model.

141

2.1. Mass conservation

142 The depth integrated mass conservation equation for the CO₂ and CH₄ can be written

$$\frac{\partial}{\partial t} (\theta_i \rho_i h_i) = -\frac{1}{r} \frac{\partial}{\partial r} (r \rho_i Q_i) \equiv R_i, \quad (2.2)$$

143 where R_i [$\text{ML}^{-2}\text{T}^{-1}$] denotes the right-hand-side of equation (2.2) and the vertically144 integrated volume fluxes, Q_i [L^2T^{-1}], are defined as

$$Q_c = \int_0^{h_c} q_c dz, \quad \text{and} \quad Q_m = \int_{h_c}^H q_m dz, \quad (2.3)$$

145 and q_i [LT^{-1}] are the respective volume fluxes.

146 2.1.1. Determination of the vertically integrated volume fluxes

147 Volume fluxes, in the context of simulating CO₂ storage problems, are generally cal-
 148 culated using Darcy's law. However, due to the lower dynamic viscosity of CO₂ at the
 149 relevant pressures of concern, it is pertinent to consider Non-Darcian losses using the
 150 Forchheimer equation (Zeng & Grigg 2006). Therefore the fluxes q_i are defined by the

151 Forchheimer equation

$$\frac{\mu_i q_i}{k k_{rg}} + \rho_i b q_i |q_i| + \frac{\partial P}{\partial r} = 0, \quad \begin{array}{l} 0 \leq z \leq h_c \quad \text{when } i=c \\ h_c < z \leq H \quad \text{when } i=m \end{array} \quad (2.4)$$

152 where k [L^2] is the reservoir permeability, k_{rg} [-] is the relative permeability of the gas,
 153 which is treated uniform and constant, b [L^{-1}] is the Forchheimer coefficient and μ_i
 154 [$ML^{-1}T^{-1}$] are the dynamic viscosities of CO_2 and CH_4 . Denoting $J = \partial P / \partial r < 0$, the
 155 appropriate positive real root can be written as

$$q_i = -\frac{k k_{rg}}{\mu_i} \left(\frac{2J}{1 + (1 - \epsilon_i J)^{1/2}} \right), \quad (2.5)$$

156 where

$$\epsilon_i = 4\rho_i b \left(\frac{k k_{rg}}{\mu_i} \right)^2. \quad (2.6)$$

157 A Maclaurin series expansion about small $\epsilon_i J$ leads to

$$q_i = -\left[1 + \epsilon_i J/4 + O(\epsilon_i^2 J^2)\right] \frac{k k_{rg} J}{\mu_i}, \quad (2.7)$$

158 from which it can be seen that the accuracy of the Darcy approximation is given by the
 159 size of the non-dimensional group $\epsilon_i J$. The issue for radially divergent (and convergent)
 160 flow problems, J becomes very large as one approaches the origin (the injection well
 161 in this case). Therefore, it is not clear whether non-Darcy effects can be ignored from
 162 information about ϵ_i alone.

163 Note that the uniform relative permeability values, k_{rg} , assumed for CO_2 and CH_4 are
 164 equivalent to the end-point relative permeability for gas in a two-phase relative perme-
 165 ability function, k_{rg0} [-] (e.g. Mathias *et al.* 2013a). In this article, for simplicity, CO_2
 166 and CH_4 are assumed to have the same relative permeabilities. In reality, they may have
 167 different relative permeabilities due to differences in interfacial tension (IFT) and con-
 168 tact angle associated with CO_2 -brine and CH_4 -brine mixtures. Bachu & Bennion (2008a)
 169 observed a set of k_{rg0} values for the same sandstone core, ranging from 0.298 to 0.526,

170 for CO₂-brine mixtures with IFT ranging from 56.2 mN/m to 19.8 mN/m, respectively
 171 (IFT was varied by increasing the fluid pressure from 1.378 MPa to 20 MPa). At 40°C
 172 and 1 MPa of pressure, the IFT for CO₂-water and CH₄-waters mixtures are around
 173 90.95 mN/m (Bachu & Bennion 2008b) and 69.06 mN/m (Ren *et al.* 2000), respectively.
 174 Therefore, relative permeabilities for CO₂-brine and CH₄-brine mixtures can be expected
 175 to be quite different. However, ignoring this difference is unlikely to significantly affect
 176 the main findings discussed hereafter.

177 The system is assumed to be initially free of CO₂. Fluid pressure is assumed initially
 178 uniform in the radial direction, at a value of P_0 at the base of the reservoir. The reservoir
 179 is confined on all sides by impermeable boundaries. Following, among others, Oldenburg
 180 (2007), Mathias *et al.* (2009), Han *et al.* (2010) and Mukhopadhyay *et al.* (2012), a
 181 constant mass flux of pure CO₂ is applied at the injection well boundary. Such conditions
 182 are described mathematically as follows:

$$\begin{aligned}
 h_c &= 0, & r_w \leq r \leq r_e, & t = 0, \\
 P &= P_0, & r_w \leq r \leq r_e, & t = 0, \\
 Q_c &= M_0/(2\pi r_w \rho_c), & r = r_w, & t > 0, \\
 Q_m &= 0, & r = r_w, & t > 0, \\
 Q_c &= 0, & r = r_e, & t > 0, \\
 Q_m &= 0, & r = r_e, & t > 0,
 \end{aligned} \tag{2.8}$$

183 where P_0 [ML⁻¹T⁻²] is the initial pressure at the base of the reservoir.

184 Differentiating equation (2.1) with respect to r gives

$$J \equiv \frac{\partial P}{\partial r} = \begin{cases} \frac{\partial}{\partial r}(P + \rho_c g h_c) - g z \frac{\partial \rho_c}{\partial r}, & 0 \leq z \leq h_c \\ \frac{\partial}{\partial r}(P - \rho_m g h_m) - g z \frac{\partial \rho_m}{\partial r}, & h_c < z \leq H \end{cases}. \tag{2.9}$$

185 showing that J is a linear function of z given the shallowness assumption that the fluid

186 densities are uniform with depth. The flux equation (2.5) can then be substituted into
 187 equation (2.3) and integrated to give

$$Q_i = -\frac{h_i k k_{rg}}{\mu_i} \left[\frac{(1 - \epsilon_i J_{i2})^{3/2} - (1 - \epsilon_i J_{i1})^{3/2}}{3\epsilon_i^2 (J_{i2} - J_{i1})/4} + \frac{2}{\epsilon_i} \right] \quad (2.10)$$

188 where

$$\begin{aligned} J_{c1} &= \frac{\partial}{\partial r} (P + \rho_c g h_c), \quad J_{c2} = J_{c1} - g h_c \frac{\partial \rho_c}{\partial r}, \\ J_{m1} &= \frac{\partial}{\partial r} (P - \rho_m g h_m) - g h_c \frac{\partial \rho_m}{\partial r}, \quad J_{m2} = J_{m1} - g h_m \frac{\partial \rho_m}{\partial r}. \end{aligned} \quad (2.11)$$

189 As written in equation (2.10), these fluxes appear singular for $\epsilon_i = 0$. However, further
 190 rearranging reveals that

$$Q_i = -\frac{h_i k k_{rg}}{\mu_i} \left(\frac{X_{i2} - X_{i1}}{J_{i2} - J_{i1}} \right), \quad X_{ij} = \frac{J_{ij}^2 (1 - 4\epsilon_i J_{ij}/3)}{(1 - \epsilon_i J_{ij})^{3/2} + 1 - 3\epsilon_i J_{ij}/2}, \quad j = 1, 2. \quad (2.12)$$

191 Also note that for slightly compressible fluids (i.e., where fluid properties do not change
 192 much with space and time) $J_{i2} - J_{i1} \rightarrow 0$, and equation (2.12) can be expanded to obtain

$$Q_i = -\frac{h_i k k_{rg}}{\mu_i} \left\{ \frac{2J_{iA}}{1 + (1 - \epsilon_i J_{iA})^{1/2}} + \frac{J_{iB}}{(1 - \epsilon_i J_{iA})^{1/2}} \left[\frac{\Upsilon_i}{12} + \frac{\Upsilon_i^3}{64} + O(\Upsilon_i^5) \right] \right\} \quad (2.13)$$

193 where

$$J_{iA} = \frac{J_{i2} + J_{i1}}{2}, \quad J_{iB} = \frac{J_{i2} - J_{i1}}{2} \quad \text{and} \quad \Upsilon_i = \frac{\epsilon_i J_{iB}}{1 - \epsilon_i J_{iA}}. \quad (2.14)$$

194 2.2. Re-casting in terms of the primary dependent variables

195 The left-hand-side of equation (2.2) can be expanded in terms of the primary dependent
 196 variables of our model, P , T and h_c , such that:

$$\theta_i \rho_i h_i \left[\left(\frac{1}{\theta_i} \frac{\partial \theta_i}{\partial P} + \frac{1}{\rho_i} \frac{\partial \rho_i}{\partial P} \right) \frac{\partial P}{\partial t} + \left(\frac{1}{\theta_i} \frac{\partial \theta_i}{\partial T} + \frac{1}{\rho_i} \frac{\partial \rho_i}{\partial T} \right) \frac{\partial T}{\partial t} + \frac{1}{h_i} \frac{\partial h_i}{\partial h_c} \frac{\partial h_c}{\partial t} \right] = R_i \quad (2.15)$$

197 where

$$\frac{\partial h_i}{\partial h_c} = \begin{cases} 1, & i = c \\ -1, & i = m \end{cases} \quad (2.16)$$

198 Imposing the constraints that the products $\theta_w \rho_w$ and $\theta_r \rho_r$ are constant and that
 199 $\sum_i \theta_i = 1$, it can be shown that for $i = c$ or m :

$$\frac{\partial \theta_i}{\partial P} = \frac{\theta_w}{\rho_w} \frac{\partial \rho_w}{\partial P} + \frac{\theta_r}{\rho_r} \frac{\partial \rho_r}{\partial P} \quad \text{and} \quad \frac{\partial \theta_i}{\partial T} = \frac{\theta_w}{\rho_w} \frac{\partial \rho_w}{\partial T} + \frac{\theta_r}{\rho_r} \frac{\partial \rho_r}{\partial T} \quad (2.17)$$

200 Now consider an isothermal compressibility, α_i [M⁻¹LT²], and an isobaric expansivity
 201 β_i [Θ^{-1}], for each of the four material components, defined as:

$$\alpha_i = \frac{1}{\rho_i} \left(\frac{\partial \rho_i}{\partial P} \right)_T \quad \text{and} \quad \beta_i = -\frac{1}{\rho_i} \left(\frac{\partial \rho_i}{\partial T} \right)_P \quad (2.18)$$

202 such that substitution of equation (2.17) into equation (2.15) leads to

$$\rho_i \left[h_i \left(\alpha_{Ei} \frac{\partial P}{\partial t} - \beta_{Ei} \frac{\partial T}{\partial t} \right) + \theta_i \frac{\partial h_i}{\partial h_c} \frac{\partial h_c}{\partial t} \right] = R_i \quad (2.19)$$

203 where

$$\alpha_{Ei} = \theta_i \alpha_i + \theta_w \alpha_w + \theta_r \alpha_r \quad \text{and} \quad \beta_{Ei} = \theta_i \beta_i + \theta_w \beta_w + \theta_r \beta_r. \quad (2.20)$$

204

2.3. Energy conservation

205 As mentioned above, pressure is assumed to be in a vertical equilibrium whilst the tem-
 206 perature and fluid properties are assumed to be vertically uniform. Consequently, heat
 207 transport is a one-dimensional process. An appropriate statement of energy conservation
 208 can therefore be written as (consider Chapter 2 of Nield & Bejan 2006):

$$\begin{aligned} \rho_{ECpE} \frac{\partial T}{\partial t} - \beta_{ET} \frac{\partial P}{\partial t} &= \frac{1}{r} \frac{\partial}{\partial r} \left(r \kappa_E \frac{\partial T}{\partial r} \right) - \left(\frac{\rho_c c_{pc} Q_c + \rho_m c_{pm} Q_m}{H} \right) \frac{\partial T}{\partial r} \\ &+ \left[\frac{(T \beta_c - 1) Q_c + (T \beta_m - 1) Q_m}{H} \right] \frac{\partial P}{\partial r} \equiv R_e \end{aligned} \quad (2.21)$$

209 where R_e [$\text{ML}^{-1}\text{T}^{-3}$] is used to denote the right-hand-side of equation (2.21) and

$$\begin{aligned}
 \rho_E c_{pE} &= \theta'_c \rho_c c_{pc} + \theta'_m \rho_m c_{pm} + \theta_w \rho_w c_{pw} + \theta_r \rho_r c_{pr}, \\
 \beta_E &= \theta'_c \beta_c + \theta'_m \beta_m + \theta_w \beta_w + \theta_r \beta_r, \\
 \kappa_E &= \theta'_c \kappa_c + \theta'_m \kappa_m + \theta_w \kappa_w + \theta_r \kappa_r,
 \end{aligned} \tag{2.22}$$

210 with c_{pi} [$\text{L}^2\text{T}^{-2}\Theta^{-1}$], β_i [Θ^{-1}], κ_i [$\text{MLT}^{-3}\Theta^{-1}$] being constant-pressure-specific-heat-
 211 capacity, thermal expansivity and thermal conductivity for the four material compo-
 212 nents, respectively and $\theta'_c = \theta_c h_c / H$ and $\theta'_m = \theta_m h_m / H$ are the depth weighted volume
 213 fractions for the CO_2 and CH_4 , respectively.

214 Note that the -1 in the $(T\beta_i - 1)Q_i$ terms in equation (2.21) comes about due to
 215 shear heating associated with fluid movement. See Chapter 2 of Nield & Bejan (2006)
 216 for further discussion on this matter.

217 Also note that the expression for κ_E represents a significant overestimate of the conduc-
 218 tivity for this composite medium. For further discussion concerning effective conductivity
 219 estimation, the reader is directed to the work of Zimmerman (1989). However, even with
 220 this upper bound estimate, conduction has been found to be of negligible effect in this
 221 context.

222 The initial and boundary conditions are:

$$\begin{aligned}
 T &= T_0, & r_w \leq r \leq r_e, & t = 0 \\
 T &= T_w, & r = r_w, & t > 0 \\
 \partial T / \partial r &= 0, & r = r_e, & t > 0,
 \end{aligned} \tag{2.23}$$

223 where T_0 [Θ] is the vertically averaged initial temperature of the reservoir and T_w [Θ] is
 224 the temperature of the injection fluid.

225

2.4. Solution by method of lines

226 Equations (2.19) and (2.21) now form a set of three, first order, quasi-linear, parabolic

227 partial differential equations that can be written as:

$$\begin{pmatrix} \rho_c h_c \alpha_{Ec} & -\rho_c h_c \beta_{Ec} & \theta_c \rho_c \\ \rho_m h_m \alpha_{Em} & -\rho_m h_m \beta_{Em} & -\theta_m \rho_m \\ -\beta_E T & \rho_E c_{pE} & 0 \end{pmatrix} \begin{pmatrix} \frac{\partial P}{\partial t} \\ \frac{\partial T}{\partial t} \\ \frac{\partial h_c}{\partial t} \end{pmatrix} = \begin{pmatrix} R_c \\ R_m \\ R_e \end{pmatrix} \quad (2.24)$$

228

229

230

231

232

233

234

Equation (2.24) represents a set of three linear equations in the time derivative of the primary variables P , T , and h_c , which can be solved to give an equation for each time derivative separately provided that the Jacobian does not vanish, which does not occur for $0 < h_c < H$. A method of lines approach is adopted, using a first-order backward difference spatial discretisation and integrating the resulting set of ordinary differential equations with respect to time using the MATLAB ODE solver, ODE15s. A similar approach was previously adopted by Mathias *et al.* (2008, 2009).

235

2.5. Fluid and rock properties

236

237

238

239

240

241

242

Because interactions between the CO₂ and CH₄, H₂O are ignored, only pure component fluid properties are required. These can be obtained using the online NIST web-book developed by Lemmon *et al.* (2013). Parameters available from the web-book include $\rho_i, c_{pi}, \mu_i, \kappa_i$ in addition to the constant-volume-specific-heat-capacity, c_{Vi} [$L^2 T^{-2} \Theta^{-1}$], and the Joule-Thomson coefficient, $\mu_{JT i}$ [$M^{-1} L T^2 \Theta$]. Invoking the Maxwell relations, compressibility, α_i , and thermal expansivity, β_i , can be obtained from (Cengel & Boles 2002, p. 627)

$$\alpha_i = \frac{T \beta_i^2}{\rho_i (c_{pi} - c_{vi})} \quad \text{and} \quad \beta_i = \frac{\rho_i c_{pi} \mu_{JT i} + 1}{T} \quad (2.25)$$

243

244

Intensive lookup tables can be developed for the three fluids for a wide range of temperatures and pressures, prior to running the numerical model. These can then be linearly

245 interpolated within the ODE solver during simultaneous solution of the aforementioned
 246 PDEs.

247 Thermal properties of the reservoir formation are taken from Oldenburg (2007) where
 248 available. These include density, $\rho_r = 2600 \text{ kg m}^{-3}$, constant-pressure-specific-heat-capacity,
 249 $c_{pr} = 1000 \text{ J kg}^{-1}\text{K}^{-1}$, thermal conductivity, $\kappa_r = 2.51 \text{ W m}^{-1} \text{ K}^{-1}$. A volumetric ther-
 250 mal expansivity of $\beta_r = 39 \times 10^{-6} \text{ K}^{-1}$ is assumed, based on the linear thermal expansion
 251 coefficient (TEC) value provided for a water saturated Berea sandstone in Table IV-2 of
 252 Somerton (1992) (also see Somerton *et al.* 1981) (note that the volumetric TEC is three
 253 times the linear TEC, see for example Zimmerman (2000)).

254 Typically, rock compressibility is parameterized by a coefficient, $c_r = (\theta_r - 1)^{-1} (d\theta_r/dP)_T$
 255 (e.g. Chen *et al.* 2006). But in the current situation, the rock compressibility is defined
 256 as $\alpha_r = \rho_r^{-1} (d\rho_r/dP)_T$. Given that the rock is static, the product $\theta_r \rho_r$ must be a con-
 257 stant. Therefore it can be shown that $\alpha_r = (1 - \theta_r) \theta_r^{-1} c_r$. Mathias *et al.* (2011b) pre-
 258 viously assumed $\theta_r = 0.8$ and $\alpha_r = 4.5 \times 10^{-10} \text{ Pa}^{-1}$. This corresponds to a value of
 259 $\alpha_r = 1.125 \times 10^{-10} \text{ Pa}^{-1}$.

260 3. Analytic Solutions

261 3.1. Heat transport

262 The above problem refers to a system whereby CO_2 displaces CH_4 . However, the thermal
 263 front resulting from CO_2 injection is generally behind the CO_2 - CH_4 interface due to heat
 264 retardation associated with the specific capacity of the host rock and residually trapped
 265 water. Furthermore, although there are large changes in pressure resulting from the in-
 266 jection process, for constant mass injection rates, these mostly occur at the beginning
 267 of injection (consider Mathias *et al.* 2011b). Consequently, when considering the devel-
 268 opment of analytical solutions for heat transport in this context, Mathias *et al.* (2010)

269 argues one can additionally assume that (1) the presence of the CH₄ can be ignored and
 270 (2) the pressure distribution is steady state. For mathematical tractability, Mathias *et*
 271 *al.* (2010) further assumes the fluid properties to be constant and uniform, and that heat
 272 conduction is negligible. In this way, equation (2.21) reduces to

$$(\theta_c \rho_c c_{pc} + \theta_w \rho_w c_{pw} + \theta_r c_{pr}) \frac{\partial T}{\partial t} = \rho_c q_c c_{pc} \left(\mu_{JTc} \frac{\partial P}{\partial r} - \frac{\partial T}{\partial r} \right) \quad (3.1)$$

273 and the profile for q_c becomes

$$q_c = \frac{M_0}{2\pi H \rho_c r}. \quad (3.2)$$

274 Substituting equation (2.4) into equation (3.1) then leads to

$$\frac{\partial T_D}{\partial \tau} + \frac{\partial T_D}{\partial \xi} = -\frac{1}{2\xi} - \frac{b_D}{(2\xi)^{3/2}} \quad (3.3)$$

275 subject to the initial and boundary conditions:

$$\begin{aligned} T_D &= 0, & \xi > 1/2, & \quad t_D = 0, \\ T_D &= T_{wD}, & \xi = 1/2, & \quad t_D > 0, \end{aligned} \quad (3.4)$$

276 where

$$\tau = \frac{M_0 c_{pc} t}{2\pi H r_w^2 (\theta_c \rho_c c_{pc} + \theta_w \rho_w c_{pw} + \theta_r c_{pr})}, \quad (3.5)$$

$$\xi = \frac{1}{2} \left(\frac{r}{r_w} \right)^2, \quad T_D = \frac{2\pi H \rho_c k k_{rg} (T - T_0)}{\mu_c \mu_{JTc} M_0}, \quad T_{wD} = \frac{2\pi H \rho_c k k_{rg} (T_w - T_0)}{\mu_c \mu_{JTc} M_0}, \quad (3.6)$$

$$b_D = \frac{k k_{rg} M_0 b}{2\pi H \mu_c r_w}. \quad (3.7)$$

277 The above problem can be solved by the method of characteristics (e.g. Knobel 1999)
 278 as follows. The complete derivative of T_D with respect to ξ can be written

$$\frac{dT_D}{d\tau} = \frac{\partial T_D}{\partial \tau} + \frac{d\xi}{d\tau} \frac{\partial T_D}{\partial \xi}. \quad (3.8)$$

279 Consider $d\xi/d\tau = 1$ such that $\xi = \tau + \xi_0$, where $\xi_0 = \xi(\tau = 0)$. By setting $d\xi/d\tau = 1$
 280 and comparing to equation (3.3) it can then be said that

$$\frac{dT_D}{d\tau} = -\frac{1}{2(\tau + \xi_0)} - \frac{b_D}{(2(\tau + \xi_0))^{3/2}}. \quad (3.9)$$

281 Integrating equation (3.9) with respect to τ , applying applying the initial condition in
 282 Equation (3.4) and then substituting $\xi_0 = \xi - \tau$ yields

$$T_D(\xi(\tau), \tau) = -\frac{1}{2} \ln\left(\frac{\xi}{\xi - \tau}\right) + \frac{b_D}{2^{1/2}} \left[\frac{1}{\xi^{1/2}} - \frac{1}{(\xi - \tau)^{1/2}} \right]. \quad (3.10)$$

283 In a similar way, the complete derivative with respect to ξ can be written

$$\frac{dT_D}{d\xi} = \frac{d\tau}{d\xi} \frac{\partial T_D}{\partial \tau} + \frac{\partial T_D}{\partial \xi} = -\frac{1}{2\xi} - \frac{b_D}{(2\xi)^{3/2}}. \quad (3.11)$$

284 Integrating equation (3.11) with respect to ξ and applying the boundary condition in
 285 equation (3.4) yields

$$T_D(\xi, \tau(\xi)) = T_{wD} - \frac{1}{2} \ln(2\xi) + b_D \left[\frac{1}{(2\xi)^{1/2}} - 1 \right]. \quad (3.12)$$

286 The two solutions are separated in the $\xi\tau$ -plane by the characteristic line, $\tau = \xi - 1/2$.
 287 It follows that the solution for the domain defined in equation (3.4) is fully described by

$$T_D = \begin{cases} -\frac{1}{2} \ln\left(\frac{\xi}{\xi - \tau}\right) + \frac{b_D}{2^{1/2}} \left[\frac{1}{\xi^{1/2}} - \frac{1}{(\xi - \tau)^{1/2}} \right], & \xi - \tau > \frac{1}{2} \\ T_{wD} - \frac{1}{2} \ln(2\xi) + b_D \left[\frac{1}{(2\xi)^{1/2}} - 1 \right], & \xi - \tau \leq \frac{1}{2} \end{cases} \quad (3.13)$$

288 When $b_D = 0$, equation (3.13) is identical to the result previously presented by Mathias
 289 *et al.* (2010), obtained by Laplace transform and assuming Darcy's law.

290 3.2. Pressure buildup

291 Disregarding statements made in the previous section, following Mukhopadhyay *et al.*
 292 (2012), consider the additional assumptions: (1) the difference between the CH₄ and
 293 CO₂ properties is negligible, (2) temperature changes are negligible and (3) the water
 294 and rock are incompressible. The mass conservation equations reduces to

$$\theta_c \rho_c \alpha_c \frac{\partial P}{\partial t} = -\frac{1}{r} \frac{\partial}{\partial r} (r \rho_c q_c) \quad (3.14)$$

295 subject to the initial and boundary conditions:

$$\begin{aligned} P_I &= P_0, & r_w \leq r \leq r_e, & t = 0, \\ \rho_c q_c &= M_0 / (2\pi H r_w), & r = r_w, & t > 0, \\ \rho_c q_c &= 0, & r = r_e, & t > 0. \end{aligned} \quad (3.15)$$

296 The above PDE is non-linear due to the dependence of ρ_c , α_c and μ_c on P . Mukhopad-
 297 hyay *et al.* (2012) linearize the above the equation by imposing a Pitzer correlation for
 298 the relationship between ρ_c and P . The linearized PDE is then solved in Laplace trans-
 299 form space and inverted back to the time-domain to obtain an analytical solution for P
 300 in the form of an integral equation, which is evaluated numerically.

301 An arguably more simple route to solution of equation (3.14) is to invoke the pseudo-

302 pressure concept of Al-Hussainy *et al.* (1996), whereby a pseudo-pressure, ψ [$\text{ML}^{-3}\text{T}^{-1}$],
 303 is defined by the derivative

$$\frac{d\psi}{dP} = \frac{\rho_c}{\mu_c} \quad (3.16)$$

304 such that the Forchheimer equation, equation (2.4), along with equation (3.14) transform
 305 to

$$\frac{(\rho_c q_c)}{k k_{rg}} + \frac{b}{\mu_c} (\rho_c q_c)^2 + \frac{\partial \psi}{\partial r} = 0, \quad (3.17)$$

$$\theta_c \alpha_c \mu_c \frac{\partial \psi}{\partial t} = -\frac{1}{r} \frac{\partial}{\partial r} (r \rho_c q_c). \quad (3.18)$$

306 Al-Hussainy *et al.* (1996) propose that the $\alpha_c \mu_c$ term in equation (3.18) can be approx-
 307 imated as a constant based on fluid properties obtained at a pressure half way between
 308 the minimum and maximum pressures being considered. Mukhopadhyay *et al.* (2012)
 309 identify this feature as a disadvantage. However, application of the pseudo-pressure con-
 310 cept in conjunction with the pseudo-time concept of Agarwal (1979) leads to a significant
 311 improvement.

312 Agarwal (1979) provides a pseudo-time, η [-], defined by the derivative

$$\frac{d\eta}{dt} = \frac{1}{\alpha_c \mu_c} \quad (3.19)$$

313 such that equation (3.18) reduces to

$$\theta_c \frac{\partial \psi}{\partial \eta} = -\frac{1}{r} \frac{\partial}{\partial r} (r \rho_c q_c). \quad (3.20)$$

314 The relationship between ψ and P is obtained by numerically evaluating the integral

$$\psi = \int_{P_0}^P \frac{\rho_c}{\mu_c} dP. \quad (3.21)$$

315 The relationship between η and t requires more creativity. The difficulty is that μ_c and
 316 α_c vary in both time and space. However, a good approximation for η can be obtained
 317 by assuming P is uniform in space, such that

$$\pi H r_e^2 \theta_c \frac{d\rho_c}{dt} \approx M_0, \quad (3.22)$$

318 which on integration yields

$$\pi H r_e^2 \theta_c (\rho_c - \rho_{c0}) \approx M_0 t, \quad (3.23)$$

319 thus providing an approximate relationship between ρ_c and t . Note that $\rho_{c0} = \rho_c(P =$
 320 $P_0)$.

321 Dividing equation (3.19) by (3.22) leads to

$$\frac{d\eta}{d\rho_c} \approx \frac{\pi H r_e^2 \theta_c}{M_0 \alpha_c \mu_c}, \quad (3.24)$$

322 which on integration yields an approximate relationship between η and ρ_c .

$$\eta \approx \frac{\pi H r_e^2 \theta_c}{M_0} \int_{\rho_{c0}}^{\rho_c} \frac{1}{\alpha_c \mu_c} d\rho_c. \quad (3.25)$$

323 Considering an identical problem but with slightly compressible fluids (e.g. Mathias *et*
 324 *al.* 2008; Mijic *et al.* 2013), the analytical solution for the problem defined by above the
 325 system of equations can be written as

$$\psi - \psi_0 = \frac{M_0}{2\pi H k k_r} \left[W + \bar{b}_D r_w \left(\frac{1}{r} - \frac{16}{5r_e} + \frac{2r}{r_e^2} - \frac{r^3}{3r_e^4} \right) \right] \quad (3.26)$$

326 where

$$W = \begin{cases} \frac{1}{2}E_1\left(\frac{\eta_e r^2}{4\eta r_e^2}\right), & \eta_0 < \eta < 0.2423\eta_e \\ \frac{2\eta}{\eta_e} + \frac{r^2}{2r_e^2} - \ln\left(\frac{r}{r_e}\right) - \frac{3}{4}, & \eta \geq 0.2423\eta_e \end{cases} \quad (3.27)$$

$$\eta_e = \frac{\theta_c r_e^2}{kk_{rg}} \quad (3.28)$$

327 and

$$\bar{b}_D = \frac{kk_{rg}M_0b}{2\pi H\bar{\mu}_c r_w} \quad (3.29)$$

328 where $\bar{\mu}_c$ is an estimate of an equivalent constant CO₂ viscosity and (Mathias & Todman
329 2010)

$$\eta_0 \approx \eta_e \left(\frac{r_w}{r_e}\right)^2 \left[\frac{(2\pi/\bar{b}_D)^2}{7 \times 10^3} + \frac{(2\pi/\bar{b}_D)^{1/2}}{3 \times 10^7} \right]^{-1}. \quad (3.30)$$

330 4. Numerical Solutions

331 Numerical solutions for the full equation were performed to explore and compare the
332 pressure and temperature response. Sensitivity analysis was undertaken around a base
333 case described by the parameters given in Table 1. These parameter are considered to be
334 typical of many depleted gas reservoirs around the UK continental shelf. The constant
335 CO₂ injection rate of 0.3 Mt/year is based on a recommendation made by Mathias *et al.*
336 (2013b), following a statistical analysis of historical oil and gas production rates in the
337 UK continental shelf. The numerical models employ a radial grid, discretised using 200
338 equal intervals in log₁₀ space, from r_w to r_e . The Forchheimer parameter, b , is calculated
339 using the correlation of Geertsma (1974)

$$b = 0.005 \theta_g^{-5.5} (kk_{rg})^{-0.5} \quad (4.1)$$

Formation thickness,	$H = 150$ m
Permeability,	$k = 100$ mD
Relative permeability,	$k_{rg} = 0.6$
CO ₂ injection rate,	$M_0 = 0.3$ Mt/year
Initial pressure,	$P_0 = 0.7$ MPa
Radial extent of reservoir,	$r_e = 3000$ m
Well radius,	$r_w = 0.1$ m
Residual water content,	$\theta_w = 0.05$
Initial temperature,	$T_0 = 35^\circ\text{C}$
Injection temperature,	$T_w = 35^\circ\text{C}$
Volume fraction of rock,	$\theta_r = 0.8$

TABLE 1. Parameter values assumed for base case.

340 Simulation output for the aforementioned base case are presented in Fig. 2. The con-
341 stant injection of CO₂ leads to an increase in fluid pressure. The CO₂ front pushes the
342 methane radially outward. Fluid pressure is greatest at the injection well. Consequently,
343 the CO₂ expands as it moves away from the injection well and experiences lower pres-
344 sures. This leads to Joule-Thomson cooling, which cools both the fluid and rock behind
345 the front. These changing temperatures and pressures lead to increases/decreases in rel-
346 evant fluid properties, which feedback to the fluid dynamics of the system.

347 Fig. 2a shows the pressure distribution (measured at the base of the reservoir, *i.e.*,
348 $P + \rho_c g h_c$) at different times. Pressure conforms to a logarithmic relationship, consistent
349 with radially symmetric problems associated with single-phase and slightly compressible
350 fluids (e.g. Mijic *et al.* 2013). The pressure wave meets the outer boundary of the reservoir,
351 at $r = r_e$, just after one year, the pressure is then seen to increase across the reservoir.

352 Fig. 2b shows temperature distributions for different times. Near to the well, temper-

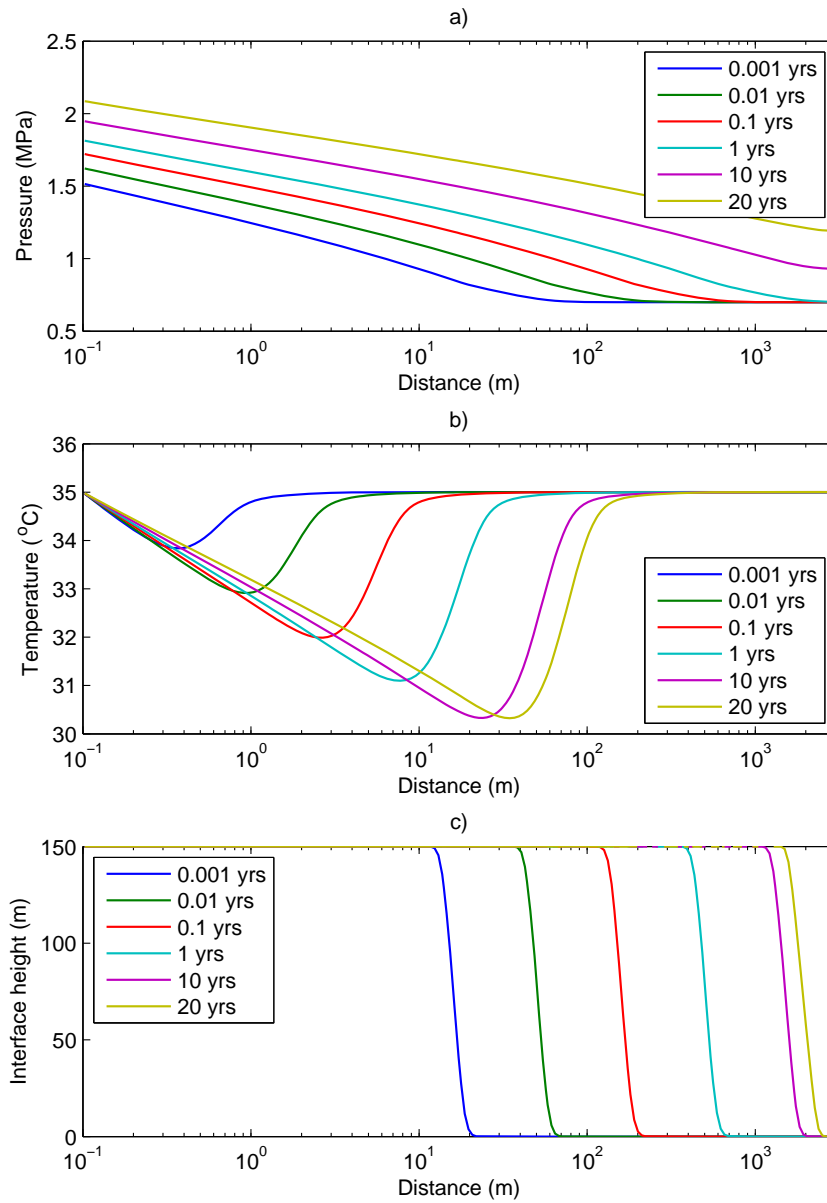


FIGURE 2. Results from the base case simulation (see Table 1) including plots of: a) pressure at the base of the reservoir, b) temperature and c) the CO_2 - CH_4 interface height against radial distance for various times, as indicated in the legends.

353 ature declines with increasing distance according to a logarithmic relationship, similar
354 to the analytical solution previously derived by Mathias *et al.* (2010). Finally, some dis-
355 tance away from the well, temperature recovers back to the initial temperature. The
356 temperature decline occurs due to the expansion of the CO₂ as it migrates away from
357 the injection well and experiences continuously decreasing pressures.

358 Fig. 2c shows the geometry of the CO₂-CH₄ interface at different times, which takes
359 the form of a moderately dispersed front. The dispersion is partly due to the gravity
360 effects associated with the diffusive-like derivative of h_c in equation (2.11). Dispersion is
361 also brought about due to the mobility difference between the CO₂ and CH₄ (consider
362 Nordbotten & Celia 2006). As discussed in Section 3.1, all the changes in temperature
363 induced by CO₂ injection reside far behind the CO₂-CH₄ interface due to the retarding
364 effect of the combined heat capacity of the rock, water and CO₂.

365 Fig. 3 presents results from a sensitivity analysis around the base case described para-
366 metrically in Table 1. Subplots a, c, e and g show plots of change in bottom hole pressure
367 in the injection well (*i.e.*, $P(r = r_w) + \rho_c g h_c - P_0$). Subplots b, d, f and h show plots of
368 temperature against distance after 20 years of injection. The solid lines are from the fully
369 coupled numerical model (hereafter referred to as non-isothermal). The circular dots are
370 from a simplified form of the numerical model whereby all fluid properties are held con-
371 stant with temperature according to the injection fluid temperature (hereafter referred
372 to as isothermal). The dashed lines are results from the analytical solutions presented in
373 Sections 3.1 and 3.2.

374 Figs. 3a and b show results looking at sensitivity to permeability. Note that an in-
375 crease in permeability has a similar effect to an increase in formation thickness and/or
376 a decrease in injection rate. Decreasing permeability leads to increased well pressures
377 and spatial pressure gradients. Consequently decreasing permeability leads to increased

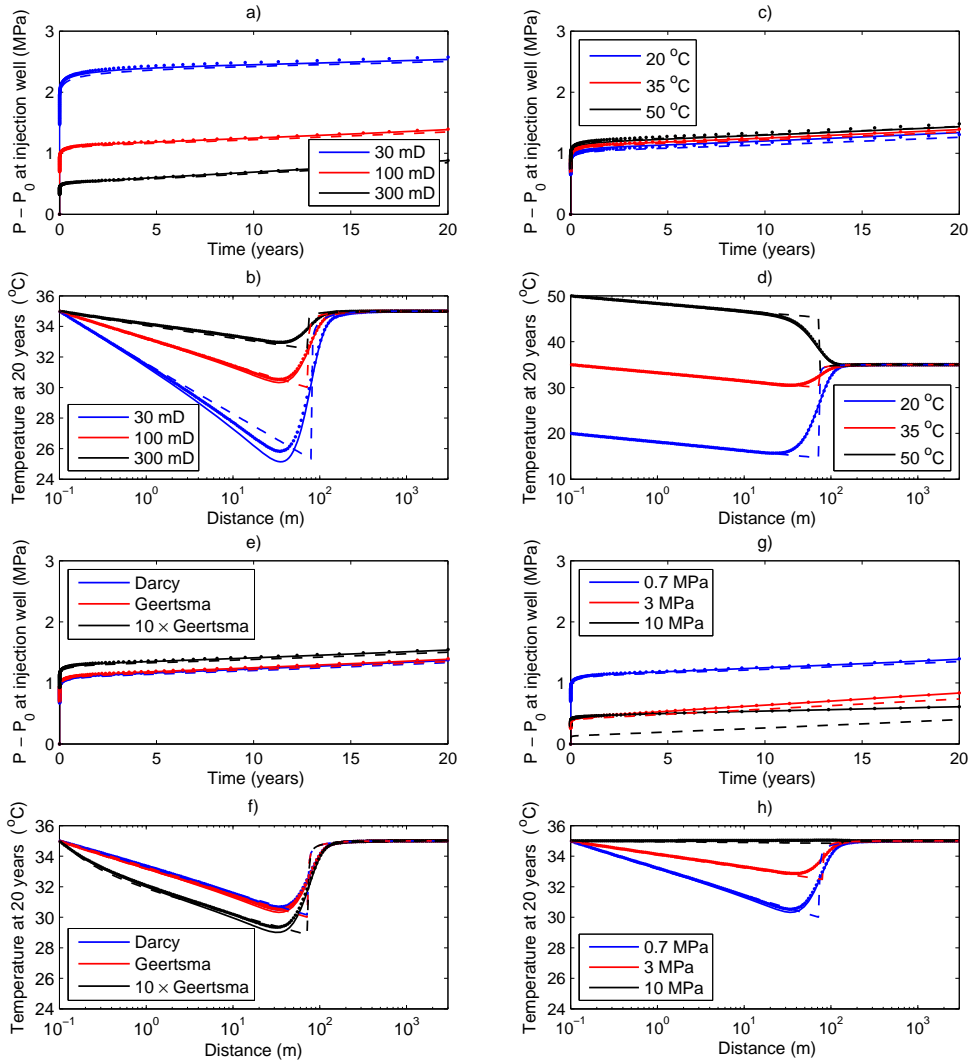


FIGURE 3. Presentation of the sensitivity analysis around the base case described in Table 1 for: a) and b) permeability, c) and d) injection fluid temperature, e) and f) non-Darcy effects, and g) and h) initial pressure, as indicated in the legends. Plots a), c), e) and g) show plots of change in bottom hole pressure against time. Plots b), d), f) and h) show plots of temperature against radial distance after 20 years of injection. The solid lines, circular dots and dashed lines are from the fully coupled model, a simplified isothermal model and the analytical solutions, respectively.

378 temperature loss away from the well. Interestingly, the difference between the isothermal
379 and non-isothermal simulation results is virtually unnoticeable, except for the estimated
380 temperature decline associated with the 30 mD model. The difference between the mod-
381 els is small because the fluid properties change very little over the temperature range of
382 30 and 35 °C at these pressures. A more significant difference is observed for the 30 mD
383 models, because the temperature decline is more severe.

384 Recall, the dashed lines are results from the analytical solutions. It is clear from Fig. 3a,
385 that the pseudo-pressure and pseudo-time approach is very effective at predicting the
386 well pressures in this context, despite its ignoring of the CH₄ fluid properties. The heat
387 transport analytical solution is also seen to be effective here (see Fig. 3b).

388 Note that previously, Mathias *et al.* (2010) observed discrepancies between numerical
389 simulation and the analytical solution (assuming Darcian flow) for temperature changes
390 greater than 5°C. It was argued that this was due to the applying of the initial pressure
391 for calculating the constant fluid properties used. Here an estimate of the well pres-
392 sure half-way through the injection period (*i.e.*, at 10 years) is used, obtained from the
393 aforementioned analytical solution for pressure buildup, in conjunction with the injection
394 fluid temperature. This is found to be very effective for all the analytical solution results
395 presented in Figs. 3b, d, f and h.

396 Recently, Ziabaksh-Ganji & Kooi (2014) argued that a notable deficiency in the an-
397 alytical solution of Mathias *et al.* (2010) (and therefore also the new solution presented
398 in Section 3.1, which uses the Forchheimer equation) was the ignoring of heating due to
399 compression. Considering Fig. 3a, it can be seen that there are initially large changes in
400 pressure with time. But after less than a small fraction of a year, the change in pressure
401 with time is dramatically reduced. In contrast, the large pressure changes with radial
402 distance persist throughout the injection period (consider again Fig. 2a). Consequently,

403 cooling due to expansion as the CO₂ moves away from the injection well has a significantly
404 more dominant effect in this context.

405 Figs. 3c and d show results from similar simulations to those used for Fig. 3a and b
406 except looking at sensitivity to injection fluid temperature. All model parameters were
407 set to the values stated in Table 1, except for the injection fluid temperature, T_w , which
408 was set to values shown in the legend. Note that the initial reservoir temperature was
409 fixed at 35 °C for all the simulations. It is apparent from Fig. 3c, that injection fluid
410 temperature, ranging from 20 to 50 °C, has very little impact on well pressure develop-
411 ment. Furthermore, it is noted that again there is very little difference between results
412 from the non-isothermal and isothermal models, and the analytical solutions are found
413 to provide a good approximation to the well-pressure and temperature response of the
414 system.

415 Figs. 3e and f explore the importance of non-Darcy effects. Results are presented,
416 again using the base case described by Table 1, using (1) Darcy's law (*i.e.*, $b = 0$), (2)
417 the Forchheimer equation with the Geertsma (1974) correlation (the base case), and (3)
418 a simulation with enhanced non-Darcy effects, obtained by multiplying the b parameter
419 obtained from the Geertsma (1974) correlation by a factor of 10. There is no noticeable
420 difference between Darcian and Forchheimer equation models using Geertsma (1974) cor-
421 relation, for both heat transport and pressure. When the non-Darcy effects are enhanced
422 by a factor of 10, a small increase in pressure is apparent along with a corresponding
423 1.5°C temperature decline. The analytical solutions for pressure and heat transport are
424 found to continue to provide good approximations in this context.

425 The Geertsma (1974) correlation has been found to correspond to large quantities of
426 empirical data (Mathias & Todman 2010). Multiplying the correlation by 10 represents
427 an upper bound on likely non-Darcy effects in this porosity range. Therefore, it can be

428 concluded that non-Darcy effects are unlikely to be a particular issue in this context.
429 Their importance can be determined in future studies by considering the dimensionless
430 group, b_D , defined in equation (3.7). For all the simulations presented in this paper,
431 with the exception of the Darcian and the enhanced non-Darcy simulations, b_D was
432 found to range from 0.07 to 0.46. The enhanced non-Darcy simulation corresponded to
433 a $b_D = 2.61$.

434 Originally it was hypothesized that non-Darcy effects would be important because of
435 the low viscosity of CO₂ at the low pressures of interest. However, equation (2.6) shows
436 that the significance of non-Darcy effects is also dependent on fluid density. The density
437 of CO₂ must also therefore be sufficiently low in this context, such that non-Darcy effects
438 are not significant here.

439 The final subplots, Figs. 3g and h, show sensitivity due to initial pressure, as indicated
440 by the values in the legend. The change in pressure in the well is found to decrease
441 with increasing initial pressure. This is due to the fluid density increasing with pressure,
442 which leads to a reduction in volumetric injection rate. The temperature change is close
443 to zero for the 10 MPa example. The temperature decline increases with decreasing initial
444 pressure. This is due to the increased pressure gradients that occur due to the increased
445 volumetric injection rate, combined with the increased Joule-Thomson coefficient of the
446 CO₂ (associated with lower pressures).

447 The performance of the analytical solution for pressure buildup is found to reduce with
448 increasing initial pressure. The main reason is that higher initial pressures correspond to
449 a larger mass of residing CH₄. Consequently, the effect of ignoring of CH₄ fluid properties
450 (in the analytical solution) becomes more important. This is less of an issue with regards
451 to the analytical solution for heat transport because temperature changes are significantly
452 reduced at higher pressures.

453 Zeidouni *et al.* (2013) previously used the analytical solution of Mathias *et al.* (2010)
454 to verify their non-isothermal simulations obtained using CMG-GEM. They noted that
455 the analytical solution underestimated cooling and heating due to the neglect of brine
456 vaporisation and CO₂ dissolution, respectively. The neglect of partial miscibility (va-
457 porisation and dissolution) between the CO₂ and the residual brine represents a limitation
458 of the numerical simulations conducted in the current study as well.

459 Andre *et al.* (2010) studied effects associated with partial miscibility in this context
460 at a reservoir pressure of 15 MPa and an injection temperature of 40°C. They found
461 temperature variation due to vaporisation and dissolution to be around 1°C to 3°C,
462 respectively. Inspection of the empirical equation for solubility limit of CO₂ in water
463 proposed by Spycher *et al.* (2003) suggests that dissolution is likely to be an order of
464 magnitude less in the context of the low pressure environments considered in this article.
465 Conversely, the work of Spycher *et al.* (2003) suggests that the reduction in pressure from
466 15 MPa to 0.7 MPa would lead to a doubling in the amount of water evaporated. However,
467 evaporation of residual water around the injection well would lead to an increase in gas
468 relative permeability. This in turn would give rise to lower pressure gradients (consider
469 Mathias *et al.* 2011b) and hence less Joule-Thomson cooling.

470 At this stage it is interesting to compare some of the above features with those as-
471 sociated with CO₂ injection into brine aquifers. For brine aquifers, the pore space is
472 predominantly filled with brine, which has a larger viscosity and lower compressibility
473 than the injected CO₂. For compartmentalized aquifers, this gives rise to a significant
474 restriction on the amount of CO₂ that can be injected, if pressures are to be constrained
475 below fracture pressure limits (Mathias *et al.* 2013a). Consequently, throughout the in-
476 jection duration, the vast majority of the reservoir pore-space continues to be occupied
477 by brine. Therefore, in contrast to depleted gas reservoirs, the compressibility of the

478 injection fluid is found to have very little impact on pressure buildup (Mathias *et al.*
479 2011a). Furthermore, because of the much larger viscosity difference between the CO₂
480 and the brine, along with the interfacial tension that develops between the CO₂-rich and
481 aqueous fluid phases, the mobility difference between the injection and reservoir fluid has
482 a much more significant impact on the pressure buildup process (Mathias *et al.* 2009,
483 2013a).

484 5. Summary and conclusions

485 In this article, a two-layer vertical equilibrium model for the injection of CO₂ into a
486 porous reservoir containing methane and water is developed. The dependent variables
487 solved for include pressure, temperature and CO₂-CH₄ interface height. In contrast to
488 previous two-layer vertical equilibrium models in this context, compressibility of all mate-
489 rial components is fully accounted for. Non-Darcy effects are also considered, which may
490 become important for low viscosity fluids. With some approximations, analytic solutions
491 for both the pressure buildup and heat transport are derived and shown to capture the
492 main dynamics and agree well with the numerical solutions.

493 The results show that, for a given injection scenario, as the initial pressure in the reser-
494 voir decreases, both pressure buildup and temperature change increase. A comparison
495 was conducted between a fully coupled non-isothermal numerical model and a simplified
496 model where fluid properties are held constant with temperature. This simplified model
497 was found to provide an excellent approximation when using the injection fluid tempera-
498 ture for calculating fluid properties, even when the injection fluid was as much as $\pm 15^\circ\text{C}$
499 of the initial reservoir temperature. The implications are that isothermal models can be
500 expected to provide useful estimates of pressure buildup in this context.

501 Non-Darcy effects were incorporated using the Forchheimer equation with the Forch-

heimer parameter, b , calculated using the Geertsma (1974) correlation. An expression
for a dimensionless Forchheimer parameter, b_D , was provided (recall equation (3.7)),
which can be used to assess the importance of non-Darcy effects. Non-Darcy effects are
likely to be negligible providing $bD < 1$. Despite the low viscosity of CO_2 at the low
pressures studied, non-Darcy effects were found to be of negligible concern throughout
the sensitivity analysis undertaken. This is because the CO_2 density is also low in this
context.

The analytical solution for pressure buildup, using the pseudo-pressure and pseudo-
time concepts of Al-Hussainy *et al.* (1996) and Agarwal (1979), respectively, was found
to provide a good approximation of the fully coupled numerical model for initial pressures
 ≤ 3 MPa. However, for higher pressures, the approximation was less accurate. The main
reason for this is that the analytical solution ignores the presence of the reservoir gas,
 CH_4 . Larger initial reservoir pressure corresponds (for a fixed volume saturation) to a
larger mass of residing CH_4 , leading the CH_4 to play a more important role concerning
pressure buildup.

The analytical solution for heat transport was found to be a good approximation
throughout the sensitivity analysis. However, it was found to be important to apply a
sensible reference pressure and temperature for calculating the CO_2 properties. Fluid
properties for this purpose were calculated using the injection fluid temperature with
an estimate of well-pressure half-way through the injection period, obtained using the
analytical solution for pressure buildup with pseudo-pressure and pseudo-time.

Acknowledgements

This work was funded by Centrica plc and a NERC Oil & Gas Catalyst award (NE/L008076/1).

REFERENCES

- 525 AFANASYEV, A. A. 2013 Multiphase compositional modelling of CO₂ injection under subcritical
526 conditions: The impact of dissolution and phase transitions between liquid and gaseous CO₂
527 on reservoir temperature. *Int. J. Greenhouse Gas Control*, **19**, 731–742.
- 528 AL-HUSSAINY, R., RAMEY JR, H. J. & CRAWFORD, P. B. 1966 The flow of real gases through
529 porous media. *J. Pet. Tech.* **577**, 363–383.
- 530 AGARWAL, R. 1979 Real gas pseudo-time – A new function for pressure buildup analysis of
531 MHF gas wells. In SPE Annual Technical Conference and Exhibition, SPE 8279–MS.
- 532 ANDRE, L., AZAROUAL, M. & MENJOZ, A. 2010 Numerical simulations of the thermal impact
533 of supercritical CO₂ injection on chemical reactivity in a carbonate saline reservoir. *Transp.*
534 *Porous Med.* **82**, 247–274.
- 535 BACHU, S. & BENNION, B. 2008a Effects of in-situ conditions on relative permeability charac-
536 teristics of CO₂-brine systems. *Environ. Geol.* **54**, 1707–1722.
- 537 BACHU, S. & BENNION, B. 2008b Interfacial tension between CO₂, freshwater, and brine in the
538 range of pressure from (2 to 27) MPa, temperature from (20 to 125) oC, and water salinity
539 from (0 to 334 000) mg/L. *J. Chem. Eng. Data* **54**, 765–775.
- 540 BARRUFET, M., BACQUET, A. & FALCONE, G. 2010 Analysis of the Storage Capacity for CO₂
541 Sequestration of a Depleted Gas Condensate Reservoir and a Saline Aquifer. *J. Canadian*
542 *Pet. Tech.* **49**, 23–31.
- 543 BENTHAM, M. & KIRBY, M. 2005 CO₂ storage in saline aquifers. *Oil Gas Sci. Tech.* **60**, 559–567.
- 544 BUCKLEY, S. E. & LEVERETT, M. C. 1942 Mechanism of fluid displacement in sands. *Trans.*
545 *AIME* **146**, 107–116.
- 546 CENGEL, Y. A. & BOLES, M. A. 2002 *Thermodynamics - An Engineering Approach. Fourth*
547 *Edition*. McGraw-Hill.
- 548 CHAPRA, S. C. & CANALE, R. P. 1998 *Numerical Methods for Engineers. Third Edition*.
549 McGraw-Hill.
- 550 CHEN, Z., HUAN, G. & MA, Y. 2006 *Computational Methods for Multiphase Flows in Porous*
551 *Media* Computational Science and Engineering Series, Vol. 2. SIAM, Philadelphia, PA.

- 552 GEERTSMA, J. 1974 Estimating the coefficient of inertial resistance in fluid flow through porous
553 media. *Old S.P.E. J.* **14**, 445–450.
- 554 GLUYAS, J. G. & HICHENS, H. M. 2003 *United Kingdom Oil and Gas Fields, Commemorative*
555 *Millennium Volume*. Geological Society, London, Memoir **20**.
- 556 HAN, W. S., STILLMAN, G. A., LU, M., MCPHERSON, B. J. & PARK, E. 2010 Evaluation of po-
557 tential nonisothermal processes and heat transport during CO₂ sequestration. *J. Geophys.*
558 *Res.* **115**, B07209.
- 559 HAN, W. S., KIM, K. Y., PARK, E., MCPHERSON, B. J., LEE, S.-Y. & M.-H. PARK 2012
560 Modeling of spatiotemporal thermal response to CO₂ injection in saline formations: Inter-
561 pretation for monitoring. *Transp. Porous Med.* **93**, 381–399.
- 562 HESSE, M. A., TCHELEPI, H. A., CANTWELL, B. J. & ORR JR, F. M. 2007 Gravity currents
563 in horizontal porous layers: transition from early to late self-similarity. *J. Fluid Mech.* **577**,
564 363–383.
- 565 HESSE, M. A., ORR, F. M. & TCHELEPI, H. A. 2008 Gravity currents with residual trapping.
566 *J. Fluid Mech.* **611**, 35–60.
- 567 KNOBEL, R. 1999 *An Introduction to the Mathematical Theory of Waves*. American Mathemat-
568 ical Society.
- 569 LEMMON, E. E., MCLINDEN, M. O. & FRIEND, D. G. 2013 Thermophysical Properties of Fluid
570 Systems. In *NIST Chemistry WebBook, NIST Standard Reference Database Number 69*,
571 National Institute of Standards and Technology, Gaithersburg MD.
- 572 LOIZZO, M., LECAMPION, B., BERARD, T., HARICHANDRAN, A. & JAMMES, L. 2009 Reusing
573 O & G depleted reservoirs for CO₂ storage: Pros and cons. In *Offshore Europe Oil & Gas*
574 *Conference & Exhibition*, SPE 124317.
- 575 MACMINN, C. W., SZULCZEWSKI, M. L. & JUANES, R. 2010 CO₂ migration in saline aquifers.
576 Part 1. Capillary trapping under slope and groundwater flow. *J. Fluid Mech.* **662**, 329–351.
- 577 MACMINN, C. W., SZULCZEWSKI, M. L. & JUANES, R. 2011 CO₂ migration in saline aquifers.
578 Part 2. Capillary and solubility trapping. *J. Fluid Mech.* **688**, 321–351.
- 579 MACROBERTS, D. T. 1962 Abandonment pressure of gas wells. In *SPE Petroleum Economics*
580 *and Valuation Symposium*, SPE-260-MS.

- 581 MATHIAS, S. A., BUTLER, A. P., & ZHAN, H. 2008 Approximate solutions for Forchheimer
582 flow to a well. *J. Hydraul. Eng.* **134**, 1318–1325.
- 583 MATHIAS, S. A., HARDISTY, P. E., TRUDELL, M. R., & ZIMMERMAN, R. W. 2009 Approximate
584 solutions for pressure buildup during CO₂ injection in brine aquifers. *Transp. Porous Media*
585 **79**, 265–284.
- 586 MATHIAS, S. A., GLUYAS, J. G., OLDENBURG, C. M., & TSANG, C. F. 2010 Analytical solution
587 for Joule–Thomson cooling during CO₂ geo-sequestration in depleted oil and gas reservoirs.
588 *Int. J. Greenhouse Gas Control* **4**, 806–810.
- 589 MATHIAS, S. A. & TODMAN, L. C. 2010 Step–drawdown tests and the Forchheimer equation.
590 *Water Resour. Res.* **46**, W07514.
- 591 MATHIAS, S. A., GLUYAS, J. G., GONZLEZ MARTNEZ DE MIGUEL, G. J., THATCHER, K. E.,
592 & ZIMMERMAN, R. W. 2011a Pressure buildup during CO₂ injection into a closed brine
593 aquifer. *Transp. Porous Media* **89**, 383–397.
- 594 MATHIAS, S. A., GLUYAS, J. G., GONZLEZ MARTNEZ DE MIGUEL, G. J. & HOSSEINI, S. A.
595 2011b Role of partial miscibility on pressure buildup due to constant rate injection of CO₂
596 into closed and open brine aquifers. *Water Resour. Res.* **47**, W12525.
- 597 MATHIAS, S. A., GLUYAS, J. G., GONZLEZ MARTNEZ DE MIGUEL, G. J., BRYANT, S. L. &
598 WILSON, D. 2013a On relative permeability data uncertainty and CO₂ injectivity estima-
599 tion for brine aquifers. *Int. J. Greenhouse Gas Control* **12**, 200–212.
- 600 MATHIAS, S. A., GLUYAS, J. G., MACKAY, E. J. & GOLDTHORPE, W. H. 2013b A statistical
601 analysis of well production rates from UK oil and gas fields – Implications for carbon
602 capture and storage. *Int. J. Greenhouse Gas Control* **19**, 510–518.
- 603 MIJIC, A., MATHIAS, S. A. & LAFORCE, T. C. 2013 Multiple well systems with non-Darcy
604 flow. *Ground Water* **51**, 588–596.
- 605 MOUTSOPOULOS, K. N., & TSIHRINTZIS, V. A. 2005 Approximate analytical solutions of the
606 Forchheimer equation. *J. Hydrol.* **309**, 93–103.
- 607 MUKHOPADHYAY, S., YANG, S. Y. & YEH, H. D. 2012 Pressure buildup during supercritical
608 carbon dioxide injection from a partially penetrating borehole into gas reservoirs. *Transp.*
609 *Porous Media* **91**, 889–911.

- 610 NIELD, D. A. & BEJAN, A. 2006 *Convection in Porous Media. Third Edition*. Springer.
- 611 NORDBOTTEN, J. M. & CELIA, M. A. 2006 Similarity solutions for fluid injection into confined
612 aquifers. *J. Fluid Mech.* **561**, 307–327.
- 613 OKWANANKE, A., YEKEEN ADEBOYE, B. & SULAIMON, L. A. 2011 Evaluation and performance
614 of natural gas storage in depleted gas reservoirs. *Petroleum & Coal* **53**, 324–332.
- 615 OLDENBERG, C. M. 2007 Joule-Thomson cooling due to CO₂ injection into natural gas reser-
616 voirs. *Energy Conv. Man.* **48**, 1808–1815.
- 617 REN, Q. Y., CHEN, G. J., YAN, W. & GUO, T. M. 2000 Interfacial tension of (CO₂ + CH₄) +
618 water from 298 K to 373 K and pressures up to 30 MPa. *J. Chem. Eng. Data* **45**, 610–612.
- 619 SINGH, A. K., GOERKE, U. J. & KOLDITZ, O. 2011 Numerical simulation of non-isothermal
620 compositional gas flow: Application to carbon dioxide injection into gas reservoirs. *Energy*
621 **36**, 3446–3458.
- 622 SINGH, A. K., BAUMANN, J., HENNINGES, J., GOERKE, U. J. & KOLDITZ, O. 2012 Numerical
623 analysis of thermal effects during carbon dioxide injection with enhanced gas recovery: a
624 theoretical case study for the Altmark gas field. *Environ. Earth Sci.* **67**, 497–509.
- 625 SOMERTON, W. H., JANAH, A. H., & ASHQAR, P. I. 1981 Thermal expansion of fluid saturated
626 rocks under stress. In *SPWLA 22nd Annual Logging Symposium* Society of Petrophysicists
627 and Well-Log Analysts. SPWLA-1981-D.
- 628 SOMERTON, W. H. 1992 *Thermal Properties and Temperature-Related Behavior of Rock/Fluid*
629 *Systems*. Developments in Petroleum Science, 37. Elsevier.
- 630 Spycher, N., Pruess, K. & Ennis-King, J. (2003), CO₂–H₂O mixtures in the geological seques-
631 tration of CO₂. I. Assessment and Calculation of Mutual Solubilities from 12 to 100 °C
632 and up to 600 bar. *Geochim. Cosmochim. Acta* **67**, 3015–3031.
- 633 ZEIDOUNI, M., NICOT, J. P. & HOVORKA, S. D. 2013 Monitoring above-zone temperature
634 variations associated with CO₂ and brine leakage from a storage aquifer. *Environmental*
635 *Earth Sciences* **In Press**.
- 636 ZENG, Z. & GRIGG, R. 2006 A criterion for non-Darcy flow in porous media. *Transp. Porous*
637 *Media* **63**, 57–69.

- 638 ZIABAKSH-GANJI, Z. & KOOI, O. 2014 Sensitivity of Joule-Thomson cooling to impure CO₂
639 injection in depleted gas reservoirs. *App. Energy* **113**, 434–451.
- 640 ZIMMERMAN, R. W. 1989 Thermal conductivity of fluid-saturated rocks. *J. Pet. Sci. Eng.* **3**,
641 219–227.
- 642 ZIMMERMAN, R. W. 2000 Coupling in poroelasticity and thermoelasticity. *J. Rock Mech. Min.*
643 *Sci.* **37**, 79–87.